

Improvement in Muon Track Reconstruction with Robust Statistics

M. G. Aartsen², R. Abbasi²⁷, Y. Abdou²², M. Ackermann⁴¹, J. Adams¹⁵,
J. A. Aguilar²¹, M. Ahlers²⁷, D. Altmann⁹, J. Auffenberg²⁷, X. Bai^{31,1},
M. Baker²⁷, S. W. Barwick²³, V. Baum²⁸, R. Bay⁷, J. J. Beatty^{17,18},
S. Bechet¹², J. Becker Tjus¹⁰, K.-H. Becker⁴⁰, M. Bell³⁸,
M. L. Benabderrahmane⁴¹, S. BenZvi²⁷, J. Berdermann⁴¹, P. Berghaus⁴¹,
D. Berley¹⁶, E. Bernardini⁴¹, A. Bernhard³⁰, D. Bertrand¹², D. Z. Besson²⁵,
G. Binder^{8,7}, D. Bindig⁴⁰, M. Bissok¹, E. Blaufuss¹⁶, J. Blumenthal¹,
D. J. Boersma³⁹, S. Bohaichuk²⁰, C. Boehm³⁴, D. Bose¹³, S. Böser¹¹,
O. Botner³⁹, L. Brayeur¹³, H.-P. Bretz⁴¹, A. M. Brown¹⁵, R. Bruijn²⁴,
J. Brunner⁴¹, M. Carson²², J. Casey⁵, M. Casier¹³, D. Chirkin²⁷,
A. Christov²¹, B. Christy¹⁶, K. Clark³⁸, F. Clevermann¹⁹, S. Coenders¹,
S. Cohen²⁴, D. F. Cowen^{38,37}, A. H. Cruz Silva⁴¹, M. Danninger³⁴,
J. Daughhetee⁵, J. C. Davis¹⁷, C. De Clercq¹³, S. De Ridder²², P. Desiati²⁷,
M. de With⁹, T. DeYoung³⁸, J. C. Díaz-Vélez²⁷, M. Dunkman³⁸, R. Eagan³⁸,
B. Eberhardt²⁸, J. Eisch²⁷, R. W. Ellsworth¹⁶, S. Euler¹, P. A. Evenson³¹,
O. Fadiran²⁷, A. R. Fazely⁶, A. Fedynitch¹⁰, J. Feintzeig²⁷, T. Feusels²²,
K. Filimonov⁷, C. Finley³⁴, T. Fischer-Wasels⁴⁰, S. Flis³⁴, A. Franckowiak¹¹,
R. Franke⁴¹, K. Frantzen¹⁹, T. Fuchs¹⁹, T. K. Gaisser³¹, J. Gallagher²⁶,
L. Gerhardt^{8,7}, L. Gladstone²⁷, T. Glüsenkamp⁴¹, A. Goldschmidt⁸,
G. Golup¹³, J. A. Goodman¹⁶, D. Góra⁴¹, D. Grant²⁰, A. Groß³⁰,
M. Gurtner⁴⁰, C. Ha^{8,7}, A. Haj Ismail²², P. Hallen¹, A. Hallgren³⁹,
F. Halzen²⁷, K. Hanson¹², D. Heereman⁴², P. Heimann¹, D. Heinen¹,
K. Helbing⁴⁰, R. Hellauer¹⁶, S. Hickford¹⁵, G. C. Hill², K. D. Hoffman¹⁶,
R. Hoffmann⁴⁰, A. Homeier¹¹, K. Hoshina²⁷, W. Huelsnitz^{16,2}, P. O. Hulth³⁴,
K. Hultqvist³⁴, S. Hussain³¹, A. Ishihara¹⁴, E. Jacobi⁴¹, J. Jacobsen²⁷,
K. Jagielski¹, G. S. Japaridze⁴, K. Jero²⁷, O. Jlelati²², B. Kaminsky⁴¹,
A. Kappes⁹, T. Karg⁴¹, A. Karle²⁷, J. L. Kelley²⁷, J. Kiryluk³⁵, F. Kislak⁴¹,
J. Kläs⁴⁰, S. R. Klein^{8,7}, J.-H. Köhne¹⁹, G. Kohnen²⁹, H. Kolanoski⁹,
L. Köpke²⁸, C. Kopper²⁷, S. Kopper⁴⁰, D. J. Koskinen³⁸, M. Kowalski¹¹,
M. Krasberg²⁷, K. Krings¹, G. Kroll²⁸, J. Kunnen¹³, N. Kurahashi²⁷,
T. Kuwabara³¹, M. Labare¹³, H. Landsman²⁷, M. J. Larson³⁶,
M. Lesiak-Bzdak³⁵, M. Leuermann¹, J. Leute³⁰, J. Lünemann²⁸, J. Madsen³³,
R. Maruyama²⁷, K. Mase¹⁴, H. S. Matis⁸, F. McNally²⁷, K. Meagher¹⁶,

*Corresponding author. Email: wellons@icecube.wisc.edu, Phone: 304-542-4464, Address: Wisconsin Institutes for Discovery, 330 N. Orchard St., Madison, WI 53715

¹Physics Department, South Dakota School of Mines and Technology, Rapid City, SD 57701, USA

²Los Alamos National Laboratory, Los Alamos, NM 87545, USA

³also Sezione INFN, Dipartimento di Fisica, I-70126, Bari, Italy

⁴Department of Physics, Sungkyunkwan University, Suwon 440-746, Korea

⁵NASA Goddard Space Flight Center, Greenbelt, MD 20771, USA

36 M. Merck²⁷, P. Mészáros^{37,38}, T. Meures¹², S. Miarecki^{8,7}, E. Middell⁴¹,
 37 N. Milke¹⁹, J. Miller¹³, L. Mohrmann⁴¹, T. Montaruli^{21,3}, R. Morse²⁷,
 38 R. Nahnhauser⁴¹, U. Naumann⁴⁰, H. Niederhausen³⁵, S. C. Nowicki²⁰,
 39 D. R. Nygren⁸, A. Obertacke⁴⁰, S. Odrowski³⁰, A. Olivas¹⁶, M. Olivo¹⁰,
 40 A. O’Murchadha¹², L. Paul¹, J. A. Pepper³⁶, C. Pérez de los Heros³⁹,
 41 C. Pfendner¹⁷, D. Pieloth¹⁹, N. Pirk⁴¹, J. Posselt⁴⁰, P. B. Price⁷,
 42 G. T. Przybylski⁸, L. Rädcl¹, K. Rawlins³, P. Redl¹⁶, R. Reimann¹,
 43 E. Resconi³⁰, W. Rhode¹⁹, M. Ribordy²⁴, M. Richman¹⁶, B. Riedel²⁷,
 44 J. P. Rodrigues²⁷, C. Rott¹⁷, T. Ruhe¹⁹, B. Ruzybayev³¹, D. Ryckbosch²²,
 45 S. M. Saba¹⁰, T. Salameh³⁸, H.-G. Sander²⁸, M. Santander²⁷, S. Sarkar³²,
 46 K. Schatto²⁸, M. Scheel¹, F. Scheriau¹⁹, T. Schmidt¹⁶, M. Schmitz¹⁹,
 47 S. Schoenen¹, S. Schöneberg¹⁰, L. Schönherr¹, A. Schönwald⁴¹, A. Schukraft¹,
 48 L. Schulte¹¹, O. Schulz³⁰, D. Seckel³¹, S. H. Seo³⁴, Y. Sestayo³⁰,
 49 S. Seunarine³³, C. Sheremata²⁰, M. W. E. Smith³⁸, M. Soiron¹, D. Soldin⁴⁰,
 50 G. M. Spiczak³³, C. Spiering⁴¹, M. Stamatikos^{17,5}, T. Stanev³¹, A. Stasik⁴¹,
 51 T. Stezelberger⁸, R. G. Stokstad⁸, A. Stöbl⁴¹, E. A. Strahler¹³, R. Ström³⁹,
 52 G. W. Sullivan¹⁶, H. Taavola³⁹, I. Taboada⁵, A. Tamburro³¹,
 53 S. Ter-Antonyan⁶, S. Tilav³¹, P. A. Toale³⁶, S. Toscano²⁷, M. Usner¹¹,
 54 D. van der Drift^{8,7}, N. van Eijndhoven¹³, A. Van Overloop²², J. van Santen²⁷,
 55 M. Vehringer¹, M. Voge¹¹, M. Vraeghe²², C. Walck³⁴, T. Waldenmaier⁹,
 56 M. Wallraff¹, R. Wasserman³⁸, Ch. Weaver²⁷, M. Wellons^{27,*}, C. Wendt²⁷,
 57 S. Westerhoff²⁷, N. Whitehorn²⁷, K. Wiebe²⁸, C. H. Wiebusch¹,
 58 D. R. Williams³⁶, H. Wissing¹⁶, M. Wolf³⁴, T. R. Wood²⁰, K. Woschnagg⁷,
 59 C. Xu³¹, D. L. Xu³⁶, X. W. Xu⁶, J. P. Yanez⁴¹, G. Yodh²³, S. Yoshida¹⁴,
 60 P. Zarzhitsky³⁶, J. Ziemann¹⁹, S. Zierke¹, A. Zilles¹, M. Zoll³⁴, B. Recht⁴²,
 61 C. Ré⁴²

62 ¹III. Physikalisches Institut, RWTH Aachen University, D-52056 Aachen, Germany

63 ²School of Chemistry & Physics, University of Adelaide, Adelaide SA, 5005 Australia

64 ³Dept. of Physics and Astronomy, University of Alaska Anchorage, 3211 Providence Dr.,
 65 Anchorage, AK 99508, USA

66 ⁴CTSPS, Clark-Atlanta University, Atlanta, GA 30314, USA

67 ⁵School of Physics and Center for Relativistic Astrophysics, Georgia Institute of
 68 Technology, Atlanta, GA 30332, USA

69 ⁶Dept. of Physics, Southern University, Baton Rouge, LA 70813, USA

70 ⁷Dept. of Physics, University of California, Berkeley, CA 94720, USA

71 ⁸Lawrence Berkeley National Laboratory, Berkeley, CA 94720, USA

72 ⁹Institut für Physik, Humboldt-Universität zu Berlin, D-12489 Berlin, Germany

73 ¹⁰Fakultät für Physik & Astronomie, Ruhr-Universität Bochum, D-44780 Bochum,
 74 Germany

75 ¹¹Physikalisches Institut, Universität Bonn, Nussallee 12, D-53115 Bonn, Germany

76 ¹²Université Libre de Bruxelles, Science Faculty CP230, B-1050 Brussels, Belgium

77 ¹³Vrije Universiteit Brussel, Dienst ELEM, B-1050 Brussels, Belgium

78 ¹⁴Dept. of Physics, Chiba University, Chiba 263-8522, Japan

79 ¹⁵Dept. of Physics and Astronomy, University of Canterbury, Private Bag 4800,
 80 Christchurch, New Zealand

81 ¹⁶Dept. of Physics, University of Maryland, College Park, MD 20742, USA

82 ¹⁷Dept. of Physics and Center for Cosmology and Astro-Particle Physics, Ohio State
 83 University, Columbus, OH 43210, USA

84 ¹⁸Dept. of Astronomy, Ohio State University, Columbus, OH 43210, USA

85 ¹⁹Dept. of Physics, TU Dortmund University, D-44221 Dortmund, Germany

- 86 ²⁰Dept. of Physics, University of Alberta, Edmonton, Alberta, Canada T6G 2E1
87 ²¹Département de physique nucléaire et corpusculaire, Université de Genève, CH-1211
88 Genève, Switzerland
89 ²²Dept. of Physics and Astronomy, University of Gent, B-9000 Gent, Belgium
90 ²³Dept. of Physics and Astronomy, University of California, Irvine, CA 92697, USA
91 ²⁴Laboratory for High Energy Physics, École Polytechnique Fédérale, CH-1015 Lausanne,
92 Switzerland
93 ²⁵Dept. of Physics and Astronomy, University of Kansas, Lawrence, KS 66045, USA
94 ²⁶Dept. of Astronomy, University of Wisconsin, Madison, WI 53706, USA
95 ²⁷Dept. of Physics and Wisconsin IceCube Particle Astrophysics Center, University of
96 Wisconsin, Madison, WI 53706, USA
97 ²⁸Institute of Physics, University of Mainz, Staudinger Weg 7, D-55099 Mainz, Germany
98 ²⁹Université de Mons, 7000 Mons, Belgium
99 ³⁰T.U. Munich, D-85748 Garching, Germany
100 ³¹Bartol Research Institute and Department of Physics and Astronomy, University of
101 Delaware, Newark, DE 19716, USA
102 ³²Dept. of Physics, University of Oxford, 1 Keble Road, Oxford OX1 3NP, UK
103 ³³Dept. of Physics, University of Wisconsin, River Falls, WI 54022, USA
104 ³⁴Oskar Klein Centre and Dept. of Physics, Stockholm University, SE-10691 Stockholm,
105 Sweden
106 ³⁵Department of Physics and Astronomy, Stony Brook University, Stony Brook, NY
107 11794-3800, USA
108 ³⁶Dept. of Physics and Astronomy, University of Alabama, Tuscaloosa, AL 35487, USA
109 ³⁷Dept. of Astronomy and Astrophysics, Pennsylvania State University, University Park,
110 PA 16802, USA
111 ³⁸Dept. of Physics, Pennsylvania State University, University Park, PA 16802, USA
112 ³⁹Dept. of Physics and Astronomy, Uppsala University, Box 516, S-75120 Uppsala, Sweden
113 ⁴⁰Dept. of Physics, University of Wuppertal, D-42119 Wuppertal, Germany
114 ⁴¹DESY, D-15735 Zeuthen, Germany
115 ⁴²Dept. of Computer Sciences, University of Wisconsin, Madison, WI 53706, USA

116 **Abstract**

117 The IceCube detector is a high-energy neutrino telescope located at the geo-
118 graphic South Pole. Neutrinos cannot be directly observed and must be inferred
119 from their interactions with other particles. These interactions sometimes gen-
120 erate a muon, which in turn emits observable light. At the energies the IceCube
121 detector is sensitive to, the neutrino and generated muon have almost parallel
122 tracks, so the neutrino track can be extrapolated from a reconstruction of the
123 muon track. However, reconstructing the muon track from the observed light is
124 challenging due to noise, light scattering in the ice medium, and the possibility
125 of simultaneously having multiple muons inside the detector.

126 This manuscript describes work on two problems: (1) the *track reconstruc-*
127 *tion* problem, in which, given a set of observations, the goal is to recover the
128 track of a muon, and (2) the *coincident event* problem, which is to determine
129 how many muons are active in the detector during a time window. Rather than
130 solving these problems by developing more complex physical models, our ap-
131 proach is to augment the detector's current models with data filters and robust
132 statistical techniques. Using the metric of median angular resolution, a standard

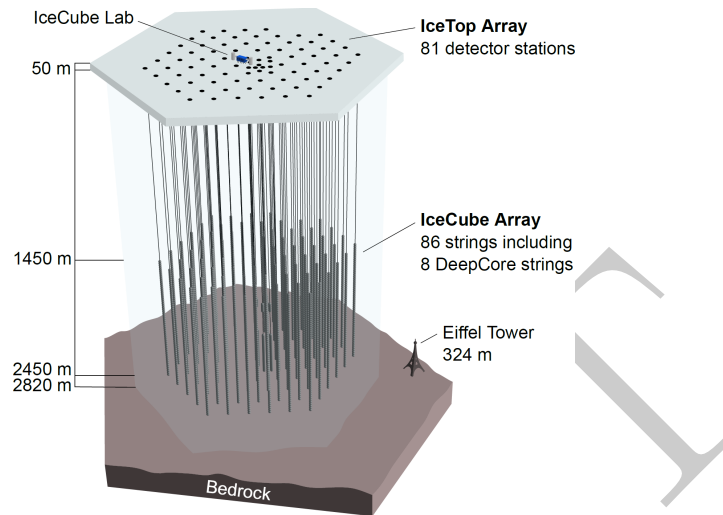


Figure 1: The IceCube neutrino detector in the Antarctic ice. A picture of the Eiffel Tower is shown for scale.

133 metric for track reconstruction, we improve the accuracy in the reconstruction
 134 direction by 13%. We also present improvements in measuring the number of
 135 muons in coincident events: we can accurately determine the number of muons
 136 98% of the time, which is an improvement of 86% over the software previously
 137 used in IceCube.

138 *Keywords:* IceCube, Track reconstruction, Neutrino telescope, Neutrino
 139 astrophysics, Robust Statistics

140 **1. Introduction**

141 The IceCube neutrino detector searches for neutrinos that are generated by
 142 the universe’s most violent astrophysical events: exploding stars, gamma ray
 143 bursts, and cataclysmic phenomena involving black holes and neutron stars [1].
 144 The detector, roughly one cubic kilometer in size, is located near the geographic
 145 South Pole and is buried to a depth of about 2.5 km in the Antarctic ice [2].
 146 The detector is illustrated in Figure 1 and a more complete description is given
 147 in Section 2.

148 When a neutrino enters the telescope, it sometimes interacts with the ice and
 149 generates a muon. The neutrino track can be extrapolated from a reconstruction
 150 of the muon track. Muons are also generated by cosmic rays, and separation
 151 of the cosmic ray muons and neutrino muons is a necessary step for neutrino
 152 analysis. This separation is challenging, as the number of observed cosmic

153 ray muons exceeds the number of observed neutrino muons by five orders of
154 magnitude [3].

155 The primary mechanism for separating the cosmic ray muons from the neu-
156 trino muons is reconstructing the muon track and determining whether the
157 muon was traveling downwards into the Earth or upwards out of the Earth.
158 Since neutrinos can penetrate the Earth but cosmic ray muons cannot, it fol-
159 lows that a muon traveling out of the Earth must have been generated by a
160 neutrino. Thus, by selecting only the muons that are reconstructed as up-
161 going, the cosmic ray muons can, in principle, be removed from the data. Since
162 the number of cosmic ray muons overwhelms the number of neutrino muons,
163 high accuracy is critical for preventing erroneous reconstruction of cosmic ray
164 muons as neutrino-induced.

165 Here, we examine two problems that arise in the separation of cosmic ray
166 muons from neutrino muons in the IceCube detector:

- 167 1. *Reconstruction*, in which the track of a muon is reconstructed from the
168 observed light at different positions and times in the detector.
- 169 2. *Coincident Event Detection*, in which we detect the number of muons
170 inside the detector, and assign observed photons to a muon.

171 Sophisticated domain models have been developed that take into account
172 the interaction of near- and far-field effects of light and mapping photon prop-
173 agation in the ice [3–5]. The current work is consequently focused on refining
174 the statistical techniques and optimizing data filtering in the online track re-
175 construction.

176 *Related Work.* Track reconstruction and coincident event detection challenges
177 are ubiquitous in particle physics [6–8], both in particle accelerators and cosmic
178 particle detectors. While the work described in this manuscript builds on the
179 previous technique developed for the IceCube detector [3], these techniques are
180 general purpose, and potentially have applications in detectors beyond IceCube.

181 *Outline.* We begin by describing the IceCube detector and track reconstruction
182 challenges in Section 2. In Section 3, we describe the reconstruction pipeline in-
183 cluding the prior IceCube software, then we present improvements to the online
184 tracking algorithm and discuss the results. Section 4 describes improvements
185 on coincident event detection, and follows a parallel structure to Section 3. We
186 conclude in Section 5.

187 2. IceCube Detector and Track Reconstruction Challenges

188 The IceCube detector is composed of 5,160 optical detectors, each composed
189 of a photomultiplier tube (PMT) and onboard digitizer [9]. The PMTs are
190 spread over 86 vertical strings arranged in a hexagonal shape, with a total
191 instrumented volume of approximately one cubic kilometer. The PMTs on a
192 given string are separated vertically by 17 m, and the string-to-string separation
193 is roughly 125 m.

194 As the muon travels through the detector, it radiates light [10], which is
 195 observed by the PMTs and divided into discrete *hits* [11]. A collection of hits
 196 is called an *event*, and if the number of hits in an event is sufficiently large, the
 197 muon track reconstruction algorithm is triggered.

198 There are several challenges for the reconstruction algorithms used in the
 199 detector. Varying optical properties of the ice affect reconstruction accuracy,
 200 the data may contain outlier hits due to uncorrelated noise, and there are finite
 201 computational resources available to tracking code run on-site.

202 *Modeling Difficulties.* The details of the ice optical properties are nontrivial to
 203 model. Light propagating through the ice is affected by scattering and absorp-
 204 tion. These effects cannot be analytically calculated and the optical properties
 205 of the ice vary with depth [5].

206 *Noise.* The noise inherent in the data is another challenge. The PMTs are so
 207 sensitive to light that they can record hits even in the absence of nearby muons.
 208 These hits can arise either from thermal background of the photocathode, or
 209 from photons generated by radioactive decay inside the PMT [9].

210 *Computational Constraints.* The reconstruction algorithms are also limited in
 211 complexity by the computing resources available at the South Pole. The track
 212 reconstruction algorithm has to process about 3,000 muons per second, algo-
 213 rithms with excessive computational demands are discouraged.

214 3. Reconstruction Improvement

215 As shown in the following, augmenting the reconstruction algorithm with
 216 some basic filters and classical data analysis techniques results in significant
 217 improvement in the reconstruction algorithm’s accuracy.

218 3.1. Prior IceCube Software

219 The muon track reconstruction process (outlined in Figure 2) starts when the
 220 number of detected hits exceeds a preset threshold and initiates data collection.
 221 After the initial data are collected, it then passes through a series of basic filters
 222 to remove obvious outliers [12].

223 This is followed by a basic reconstruction algorithm, *linefit*, which finds the
 224 track that minimizes the sum of the squares of the distances between the track
 225 and the hits. More formally, assume there are N hits; denote the position
 226 and time of the i th hit as \vec{x}_i and t_i , respectively. Let the reconstructed muon
 227 track have a velocity of \vec{v} , and let the reconstructed track pass through point
 228 \vec{x}_0 at time t_0 . Then linefit reconstruction solves the *least-squares* optimization
 229 problem

$$\min_{t_0, \vec{x}_0, \vec{v}} \sum_{i=1}^N \rho_i(t_0, \vec{x}_0, \vec{v})^2, \quad (1)$$

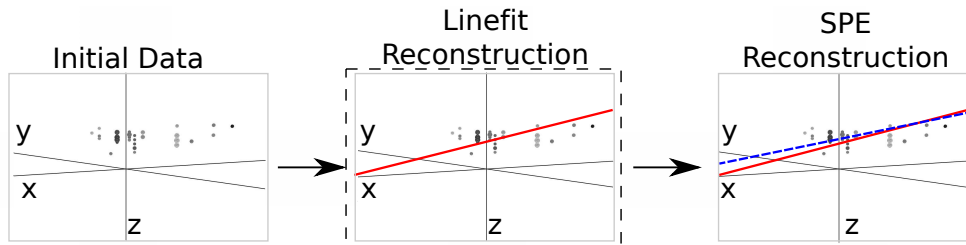


Figure 2: The reconstruction pipeline used to process data in the IceCube detector. After initial data are collected, it is then processed by some basic noise filters, which remove clear outliers. This cleaned data are processed by a basic reconstruction algorithm (solid line), which is used as the seed for the more sophisticated reconstruction algorithm (dashed line). The sophisticated reconstruction is then evaluated as a potential neutrino. The work presented in this manuscript makes changes to the basic reconstruction step (indicated by the dashed box).

230 where

$$\rho_i(t_0, \vec{x}_0, \vec{v}) = \|\vec{v}(t_i - t_0) + \vec{x}_0 - \vec{x}_i\|_2. \quad (2)$$

231 Linefit is primarily used to generate an initial track or *seed* for a more sophis-
 232 ticated reconstruction.

233 The reconstruction algorithm for the sophisticated reconstruction is *Single-*
 234 *Photo-Electron-Fit (SPE fit)* [3]. SPE fit uses the least-squares reconstruction,
 235 the event data, and a parameterized probability distribution function of scatter-
 236 ing in ice [3] to reconstruct the muon track.

237 3.2. Algorithm Improvement

238 SPE fit is dependent on the seed. Given a seed that is inaccurate by 6° or
 239 more, SPE fit typically cannot recover, and produces a reconstruction with the
 240 same level of inaccuracy as the seed track. In addition, the likelihood space for
 241 SPE fit can contain multiple local maxima, so improving the accuracy of a seed
 242 that is already near the true solution improves the accuracy of SPE fit. Thus,
 243 we focus here on improving the quality of the seed.

244 As indicated in Equation 1, a least-squares fit models the muon as a single
 245 point moving in a straight line, and hits are penalized quadratically in their
 246 distance from this line. Thus there is an implicit assumption in this model:
 247 that all the hits will be near the muon. This assumption has two pitfalls:

- 248 1. It ignores the scattering effects of the ice medium. Some of the photons can
 249 scatter for over a microsecond, which means that when they are recorded
 250 by a PMT, the muon will be over 300 m away.
- 251 2. While the noise reduction steps remove most of the outlier noise, the noise
 252 hits that survive can be far from the muon. Since these outliers are given
 253 quadratic weight, they exert a huge influence over the model.

254 The first pitfall occurs because the model is incomplete and does not accu-
 255 rately model the data, and the second demonstrates that the model is not robust

256 to noise. The solution to this is twofold: improve the model and increase the
 257 noise robustness by replacing least squares with robust statistical techniques.

258 3.2.1. Improving the Model

259 The least-squares model does not model the scattering, and thus hits gen-
 260 erated by photons that scattered for a significant length of time are not useful
 261 predictors of the muon’s position. We found that a basic filter could identify
 262 these scattered hits, and improve accuracy by of almost a factor of two by
 263 removing them from the dataset.

264 More formally, for each hit h_i , the algorithm looks at all neighboring hits
 265 within a neighborhood of r , and if there exists a neighboring hit h_j with a time
 266 stamp that is t earlier than h_i , then h_i is considered a scattered hit, and is
 267 not used in the basic reconstruction algorithm. Optimal values of r and t were
 268 found to be 156 m and 778 ns by tuning them on simulated muon data.

269 3.2.2. Adding Robustness to Noise

270 As described in equation 1, the least squares model gives outliers quadratic
 271 weight, whereas we would prefer that outliers had zero weight. There are robust
 272 models in classical statistics designed to marginalize outliers. We experimented
 273 replacing the least-squares model with a Huber fit [13], which improved the
 274 reconstruction accuracy.

275 More formally, we replace Equation 1 with the optimization problem:

$$\min_{t_0, \vec{x}_0, \vec{v}} \sum_{i=1}^N \phi(\rho_i(t_0, \vec{x}_0, \vec{v})), \quad (3)$$

276 where the Huber penalty function $\phi(\rho)$ is defined as

$$\phi(\rho) \equiv \begin{cases} \rho^2 & \text{if } \rho < \mu \\ \mu(2\rho - \mu) & \text{if } \rho \geq \mu \end{cases}. \quad (4)$$

277 Here, $\rho_i(t_0, \vec{x}, \vec{v})$ is defined in Equation 2 and μ is a constant calibrated to the
 278 data (on simulated muon events, the optimal value of μ is 153 m).

279 The Huber penalty function has two regimes. In the near-hit regime ($\rho < \mu$),
 280 hits are assumed to be strongly correlated with the muon’s track, and the Huber
 281 penalty function behaves like least squares, giving these hits quadratic weight.
 282 In the far-hit regime ($\rho \geq \mu$), hits are given linear weights as they are more
 283 likely to be noise.

284 In addition to its attractive robustness properties, the Huber fit’s weight
 285 assignment also has the added benefit that it inherently labels points as outliers
 286 (those with $\rho \geq \mu$). Thus, once the Huber fit is computed, we can go one step
 287 farther and simply remove the labeled outliers from the dataset. A better fit is
 288 then obtained by computing the least-squares fit on the data with the outliers
 289 removed. The entire algorithm has a mean runtime that is approximately six
 290 times slower than Linefit’s mean runtime.

Table 1: Median angular resolution (degrees) for reconstruction improvements. The first line is the accuracy of the prior least-squares model, and the subsequent lines are the accuracy measurements from cumulatively adding improvements into the basic reconstruction algorithm.

Algorithm	θ_{med}
Linefit Reconstruction (Least-Squares)	9.917
With Addition of Logical Filter	5.205
With Addition of Huber Regression	4.672
With Addition of Outlier Removal	4.211

3.3. Results

The goal is to improve the accuracy of the reconstruction in order to better separate neutrinos from cosmic rays. Thus we present three measurements: (1) the accuracy change between linefit and the new algorithm, (2) the accuracy change when SPE is seeded with the new algorithm instead of linefit, and (3) the improvement in separation between neutrinos and cosmic rays.

To measure the improvement generated by the changes, we use the metric of *median angular resolution* θ_{med} , which is a standard metric within the collaboration. The angular resolution of a reconstruction is the arc-distance between the reconstruction and the true track. The dataset is drawn from simulated neutrino data designed to be similar to that observed by the detector.

We can improve the median angular resolution of the basic reconstruction by 57.6%, as shown in Table 1. Seeding SPE with the improved basic reconstruction generates an improvement in the angular resolution of 12.9%. These improvements in the reconstruction algorithm result in 10% fewer atmospheric muons erroneously reconstructed as up-going, and 1% more muons correctly reconstructed as up-going.

4. Coincident Event Improvements

In the second study, we look at the problem of determining when more than one muon has entered the detector. In the most common case, a single muon will pass through the detector and generate an event before exiting. These events are processed by the pipeline described in Figure 2. However, for roughly 9% of the events collected by the data collection algorithm, more than one muon will be passing through the detector simultaneously, an occurrence known as a *coincident event*.

One of the primary sources of background noise in IceCube analyses is coincident background muons that have been erroneously reconstructed as neutrinos. To see why this occurs, consider the coincident event shown in Figure 3. There are two clear groups of hits; however, the reconstruction algorithm treats them as a single group, resulting in an erroneous reconstruction. In the ideal case, the reconstruction algorithm would identify coincident events and split them, as in Figure 4.

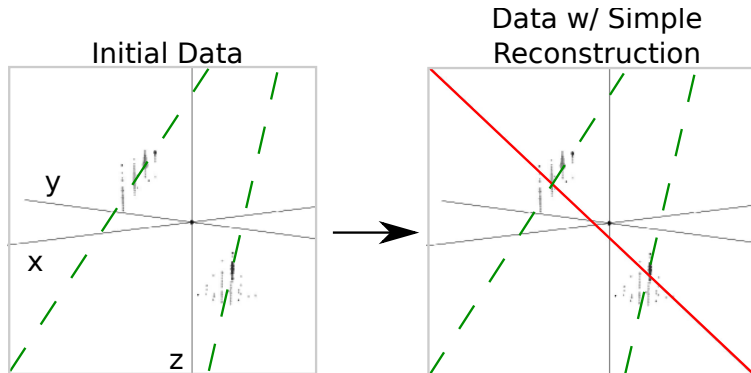


Figure 3: In this example, an event that is clearly composed of two muons (actual tracks shown as dashed lines) is treated as a single muon, and thus the reconstruction (solid line) is inaccurate.

323 The challenge in this example is determining the number of muons in an
 324 event. Our studies show that a simple spatial clustering algorithm can solve
 325 this classification problem with less than 2% error.

326 4.1. Prior IceCube Software

327 Coincident events have been a concern in the IceCube analysis [14] for years,
 328 and some software has been developed to handle coincident events. As a baseline
 329 of comparison, we use the *TTrigger* software, which is described in [15].

330 4.2. Algorithm Improvement

331 Here we present a proximal clustering algorithm. The intuition in proximal
 332 clustering is that points local in space and time are probably from the same
 333 muon. The proximal clustering algorithm iterates through each pair of hits
 334 (i, j) and builds an adjacency matrix \mathbf{A} as

$$\mathbf{A}_{ij} = \begin{cases} 1 & \text{if } \|\Delta x^2 + \Delta y^2 + \Delta z^2 + (c\Delta t)^2\|_2 \leq \alpha, \\ 0 & \text{otherwise} \end{cases} \quad (5)$$

335 where $\Delta x, \Delta y, \Delta z$ and Δt are the space and time differences between the pair
 336 of hits, and α is tuned to the data (in this application, the optimal value of
 337 α is 450 m). The clustering can be recovered by extracting the connected
 338 components of the graph defined by \mathbf{A} . A connected component of a graph is a
 339 subgraph such that there exist a path between any two vertices of this subgraph.

340 4.2.1. Improving the Model

341 When implemented naively, proximal clustering succeeded for the majority
 342 of the events, but failed if there was a gap in the muon track, which can occur
 343 when the muon travels through dusty ice. If there is a significantly large gap,
 344 the algorithm erroneously separates the hits into two clusters.

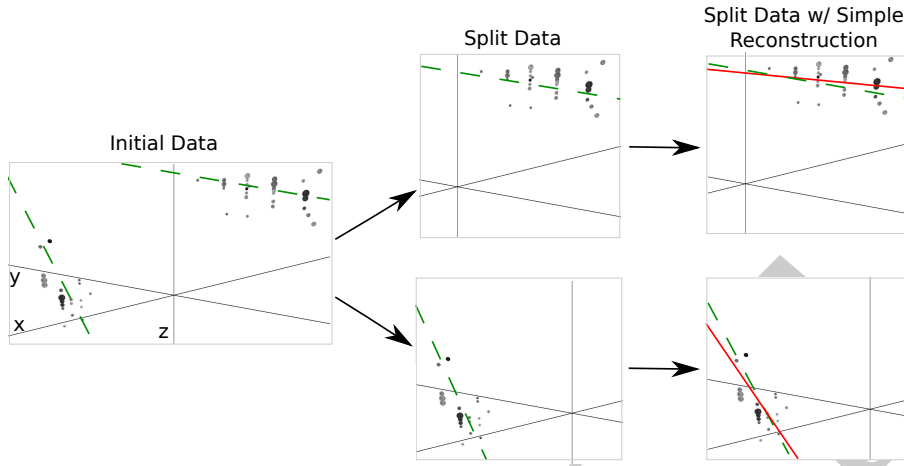


Figure 4: Ideally, the detector would split coincident events before computing the reconstruction. Splitting the event results in more accurate reconstructions (reconstructions shown as solid lines, true muon tracks shown as dashed lines). Note the difference in the reconstructions compared with Figure 3.

345 To get around this, an additional heuristic is added, *track connecting*. Af-
 346 ter the data segmentation is finished, track connecting determines if separate
 347 clusters should be combined. It computes the mean position and time of each
 348 cluster, and connects a hypothetical muon track T between each pair of sub-
 349 spaces.

350 It checks if the speed s of the hypothetical track is within 25% of the speed
 351 of light c , and it checks that the mean distance between hits and T in both
 352 clusters is less than 60 m. If T passes both checks, the clusters are combined.

353 4.2.2. Adding Robustness to Noise

354 Proximal clustering is susceptible to noise. Noise hits close to two disjoint
 355 tracks will be considered adjacent to both tracks, and thus can connect the two
 356 tracks in the adjacency matrix.

357 One heuristic that worked well at mitigating this problem was to not use
 358 all the hits in building the adjacency matrix. During data collection, some hits
 359 are flagged as having a *local coincidence condition*, which indicates that both
 360 they and a neighboring PMT reported a hit. These hits have a high probability
 361 of not being noise hits, and thus exclusively using them to build the adjacency
 362 matrix mitigates the problem of erroneously connecting two tracks.

363 After the proximal clustering algorithm has extracted the tracks from the
 364 adjacency matrix, the hits not used in the construction of the adjacency matrix
 365 are simply assigned to the closest reconstructed track.

366 4.3. Results

367 There were two competing goals for coincident event detection algorithms:
 368 the algorithm should be conservative enough that events containing single tracks

Table 2: Error Rates for Classification Algorithms

Algorithm	$E_{\text{Single}} \%$	$E_{\text{Multiple}} \%$	$E_{\text{tot}} \%$
Trivial	0.0	100.0	8.3
TTrigger	11.5	31.8	13.2
Proximal clustering	0.2	18.9	1.8

369 are not erroneously split, and aggressive enough that a useful fraction of coin-
370 cident events are split correctly. Erroneously discarding events containing neu-
371 trinos is worse than erroneously allowing additional noise into the data pool,
372 as noise can be eliminated by future filtering of the data pool. Our algorithm
373 is tuned to keep almost all of the single events correctly unsplit, while still
374 correctly splitting 80% of the coincident events.

375 4.3.1. Measurements

376 We modified the reconstruction pipeline shown in Figure 2, in between the
377 noise cleaning and the basic reconstruction, by adding a step for coincident event
378 detection, as shown in Figure 4. This step takes cleaned data and attempts to
379 classify the event as a single-track or multiple-track event.

380 We ran each algorithm on two datasets of simulated data. One dataset
381 comprised single-muon events, and the other dataset comprised multiple-muon
382 events. In each dataset, we measured the classification error E , which is the
383 fraction of events that were misclassified. To get a global measurement, we
384 compute the *total error* E_{tot} , defined as

$$E_{\text{tot}} = w_{\text{Single}} E_{\text{Single}} + w_{\text{Multiple}} E_{\text{Multiple}}. \quad (6)$$

385 For computing E_{tot} , we use $w_{\text{Single}} = 0.917$ and $w_{\text{Multiple}} = 0.083$, which is
386 the frequency in which single-muon and multiple-muon events appear in data
387 simulating the distribution of events that trigger the reconstruction algorithm.

388 We present the results for the coincident event problem by measuring how
389 well each algorithm performs at determining the number of subspaces in an
390 event.

391 There are two natural comparisons for the work: the prior software TTrigger,
392 as well as the trivial algorithm, which always classifies each event as a single-
393 track event. Clearly, the latter will always get the single-track events correct,
394 and always get the multiple-track events wrong. We provide a comparison of
395 these techniques in Table 2. As shown, the new algorithm classifies the number
396 of muons in the detector 86% better than TTrigger.

397 5. Conclusions

398 We found that significant improvements can be achieved in the IceCube’s on-
399 line track reconstruction by employing some classical data analysis algorithms.
400 Optimizing data filtering and refining the least-square model have led to signif-
401 icant improvements in the accuracy of the reconstruction direction. The new

402 reconstruction software is fast enough to run on-site, and is now included in all
403 IceCube analyses.

404 We also looked at the problem of determining the number of muons in the
405 detector. We found that proximal clustering with some basic heuristics could
406 correctly determine whether an event contained a single muon or multiple muons
407 with less than 2% error, yielding an 86% improvement over the prior software.

408 References

- 409 [1] IceCube Collaboration, IceCube webpage, <http://icecube.wisc.edu/>.
- 410 [2] IceCube Collaboration, First year performance of the IceCube neutrino
411 telescope, *Astroparticle Physics* 26 (3) (2006) 155–173.
- 412 [3] IceCube Collaboration, Muon track reconstruction and data selection tech-
413 niques in AMANDA, *Nuclear Instruments and Methods in Physics Re-*
414 *search Section A* 524 (2004) 169–194.
- 415 [4] IceCube Collaboration, Measurement of South Pole ice transparency with
416 the IceCube LED calibration system IceCube Collaboration, *Nuclear In-*
417 *struments and Methods in Physics Research Section A* (2013) 73–89.
- 418 [5] The AMANDA Collaboration, Optical properties of deep glacial ice at the
419 south pole, *Journal of Geophysical Research* 111 (D13) (2006) D13203.
- 420 [6] ATLAS Collaboration, Tracking and vertexing with the ATLAS detector at
421 the LHC, *Nuclear Instruments and Methods in Physics Research Section A:*
422 *Accelerators, Spectrometers, Detectors and Associated Equipment* 650 (1)
423 (2011) 218–223.
- 424 [7] R. S. Chivukula, M. Golden, E. H. Simmons, Multi-jet physics at hadron
425 colliders, *Nuclear Physics B* 363 (1) (1991) 83–96.
- 426 [8] S. Ellis, J. Huston, K. Hatakeyama, P. Loch, M. Tönnesmann, Jets in
427 hadron–hadron collisions, *Progress in Particle and Nuclear Physics* (60)
428 (2008) 484–551.
- 429 [9] IceCube Collaboration, Calibration and characterization of the IceCube
430 photomultiplier tube, *Nuclear Instruments and Methods in Physics Re-*
431 *search Section A* 618 (2010) 139–152.
- 432 [10] IceCube Collaboration, An improved method for measuring muon energy
433 using the truncated mean of dE/dx , *Nuclear Instruments and Methods in*
434 *Physics Research Section A* 703 (1) (2012) 190–198.
- 435 [11] IceCube Collaboration, The icecube data acquisition system: Signal cap-
436 ture, digitization, and timestamping, *Nuclear Instruments and Methods in*
437 *Physics Research Section A* 601 (3) (2009) 294–316.

- 438 [12] M. Ackermann, Searches for signals from cosmic point-like sources of high
439 energy neutrinos in 5 years of AMANDA-II data, Ph.D. thesis, Humboldt-
440 Universität zu Berlin (2006).
- 441 [13] S. Boyd, L. Vandenberghe, Convex Optimization, Cambridge University
442 Press, 2009.
- 443 [14] IceCube Collaboration, Measurement of the atmospheric neutrino energy
444 spectrum from 100 GeV to 400 TeV with IceCube, Physical Review D
445 83 (1).
- 446 [15] D. Chirkin, Measurement of the atmospheric neutrino energy spectrum
447 with IceCube, Proceedings of the 31st ICRC.

DRAFT